Effects of Roof Shape and Roof Pitch on Extreme Wind Fragility for Roof Sheathing

Shuochuan Meng, S.M.ASCE[1]; Caroline J. Williams, S.M.ASCE[2]; Rachel A. Davidson, A.M.ASCE[3]; and Ertugrul Taciroglu, M.ASCE[4]

Abstract: Wind fragility curves for roof sheathing were developed for single-family building models to investigate the effects of roof shape and roof pitch on the wind performance of roof sheathing. For gable roofs, it was found that more complex roof shapes are more likely to suffer roof sheathing damage when subjected to high winds. The probability of no roof sheathing failure can be up to 36% higher for a simple gable roof than for a complex gable roof. For hip roofs with different configurations, variation in roof shape has minimal effect on roof sheathing fragility. Roof pitch effects were also evaluated for 10 pitch angles, ranging from 14° to 45°. Results suggest that for roof pitches smaller than 27°, the effects of this angle are more substantial on the performance of gable roofs than on hip roofs. For gable roofs, the probability of no roof sheathing failure can be up to 23% higher for a 23° roof pitch than that for an 18° roof pitch. Furthermore, the inclusion of complex roof shapes in a regional hurricane loss model for New Hanover County, North Carolina, accounted for a 44% increase in estimated annual expected losses from roof sheathing damages compared to a scenario in which all roofs are assumed to have rectangular roof shapes. Therefore, to avoid an underestimation of roof damages due to high-wind impact, the inclusion of complex roof geometries in hurricane loss modeling is strongly recommended. **DOI: 10.1061/JSENDH.STENG-11846.**

Introduction

Damage to the roofs of single-family residential buildings is frequently observed in extreme wind hazard events. Uplift pressure acting on roofs can remove roof sheathing panels from roof framing. Loss of a single piece of the roof sheathing can cause rainwater penetration, resulting in severe interior damage and corresponding content losses (Sparks et al. 1994). Moreover, the loss of roof sheathing can induce sudden internal pressurization and affect the wind pressure applied on other building components (Liu and Saathoff 1981). Hence, accurately predicting the performance of roof sheathing is critical for damage and loss estimation of the whole building structure.

Based on functional and aesthetic needs, most single-family residential buildings in the United States have nonrectangular footprints with resulting complex roof configurations. The roof pitch for residential buildings can vary from 3:13 (14°) to 12:12 (45°). Existing wind vulnerability models, including the FEMA HAZUS-MH model (Vickery et al. 2006) and the Florida Public Hurricane Loss Model (FPHLM) (Pinelli et al. 2011; Hamid 2019), only adopt archetype building models with rectangular footprints and a single roof pitch. Variations of roof shape and roof pitch have not been considered in the regional loss estimation in these existing models to date.

Previous research on the reliability of roof sheathing subjected to high wind has mostly focused on simple roof shapes with rectangular building plans (Ellingwood et al. 2004; Lee and Rosowsky 2005; Li 2005; van de Lindt and Dao 2009). Only a limited number of studies considered building models with complex roof shapes and nonrectangular building plans (Amini and van de Lindt 2014; Masoomi et al. 2018; Stewart et al. 2018). Amini and van de Lindt (2014) developed tornado fragilities for four complex gable-roofed buildings and one simple hip-roofed building using wind loads calculated based on ASCE 7-10 (ASCE 2010). Masoomi et al. (2018) conducted fragility analysis on the same set of building models considering both straight-line winds and tornadoes using ASCE 7-10 (ASCE 2010) and ASCE 7-16 (ASCE 2016). Stewart et al. (2018) developed fragility curves for metal roof sheeting on a complex hip-roofed building using wind pressure data obtained from wind tunnel tests. Nevertheless, due to the limited number of building models, the effects of roof shape and roof pitch on roof sheathing fragilities remain unclear.

Recent advancements in remote sensing and computer vision have provided powerful tools to extract detailed building geometry from three-dimensional point cloud data and two-dimensional aerial images. Kashani et al. (2016) introduced a lidar-based methodology for extracting roof geometry and developing detailed fragility models for buildings with complex roof shapes. El Merabet et al. (2015) applied machine learning techniques to model roof ridges and segment roofs from aerial images. The enriched building data can facilitate the development of site-specific roof fragility models, which can then be applied to regional hurricane loss models. Therefore, the inclusion of more complex roof geometries that reflect ground conditions has the potential to provide more realistic loss estimates.

This study adds to the existing literature by quantitatively evaluating the effects of roof shape and roof pitch on roof sheathing fragility for single-family houses with rectangular and nonrectangular

[1]Graduate Student, Dept. of Civil and Environmental Engineering, Univ. of California, Los Angeles, CA 90095. ORCID: https://orcid.org/0000-0001-7651-6896

[2]Graduate Student, Dept. of Civil and Environmental Engineering, Univ. of Delaware, Newark, DE 19716. ORCID: https://orcid.org/0000-0003-1918-7664

[3]Professor, Dept. of Civil and Environmental Engineering, Univ. of Delaware, Newark, DE 19716. ORCID: https://orcid.org/0000-0002-6061-5985

[4]Professor, Dept. of Civil and Environmental Engineering, Univ. of California, Los Angeles, CA 90095 (corresponding author). ORCID: https://orcid.org/0000-0001-9618-1210. Email: etacir@ucla.edu

Note. This manuscript was submitted on July 7, 2022; approved on March 1, 2023; published online on May 12, 2023. Discussion period open until October 12, 2023; separate discussions must be submitted for individual papers. This paper is part of the ***Journal of Structural Engineering***, © ASCE, ISSN 0733-9445.

roof shapes using ASCE 7-16 wind loading (ASCE 2016). Additionally, the study compares the expected annual roof sheathing losses when a simple roof inventory (only rectangular roof shapes) or a complex roof inventory (rectangular and nonrectangular) is utilized in a regional component-based loss model, using New Hanover County, North Carolina, as a case study.

Following a description of the building models used, the fragility modeling methodology is explained. Next, the fragility curves for building models with different roof shapes and roof pitches are presented, and the results are discussed in terms of failure probabilities and fragility parameters. Then the impact of roof shapes on regional loss estimation is evaluated using a case study. In the end, the limitations of the analysis are discussed, and suggestions on roof modeling for wind vulnerability models are provided.

Building Models

Two sets of building models were used to evaluate roof type and roof pitch effects on roof sheathing fragility, respectively. The first set includes 47 building models (five rectangular gable-roofed, 18 complex gable-roofed, one rectangular hip-roofed, and 23 complex hip-roofed cases), designated Types 1–47 (Figs. 1 and 2). The 47 building models were classified into Groups 1–12 based on roof complexity, with the number of ridgelines for gable roofs (one to five) and the number of roof corners for hip roofs (four to nine) used as the primary features representing the roof complexity. Groups 1 and 3–6 represent buildings with rectangular gable roofs and complex gable roofs, respectively. Groups 7 and 8–12 represent buildings with rectangular hip roofs and complex hip roofs, respectively. Building models were designed to have similar plan areas and dimensions. Roof configurations and building properties of building models were developed based on common practice in residential construction. They are intended to be representative of most single-family houses in hurricane-prone areas of the United States. Table 1 presents the properties of Building Model Set 1. The building dimensions and roof configuration for Structure Type 6 are shown in Fig. 3 as an example. Roof dimensions and panel layouts for gable- and hip-roofed building models are shown in Figs. 1 and 2, respectively.

The second set of 40 building models includes four baseline structures, designated Types A–D, with 10 different roof pitches (Fig. 4). The baseline structures are considered representative of gable- and hip-roofed buildings with rectangular and nonrectangular footprints. The roof pitches vary from 3:12 (14°) to 12:12 (45°), covering commonly used pitch angles in residential buildings. Building properties for the four baseline models are summarized in Table 2.

Fragility Modeling Methodology

Damage States

The failure of roof sheathing due to wind load is usually caused by negative wind pressure (suction) acting on the panel, which causes multiple nail withdrawals and leads to the removal of roof sheathing from roof framing. The limit state for the uplift of an individual roof sheathing panel can be expressed by

$$g(R, W, D) = R - (W - D) \tag{1}$$

where R = uplift capacity of roof sheathing; W = uplift wind load acting on the roof sheathing; and D = dead load. The failure of individual roof sheathing is defined as $g(\cdot) < 0$. For the fragility of a roof sheathing system that consists of multiple roof panels, five damage states were considered, which are consistent with previous studies (Lee and Rosowsky 2005; Amini and van de Lindt 2014): (DS1) no roof sheathing failure; (DS2) one roof sheathing panel fails; (DS3) more than one, and less than or equal to 10% of roof sheathing panels fail; (DS4) more than 10%, and less than or equal to 25% of roof sheathing panels fail; and (DS5) more than 25% of roof sheathing panels fail.

Fragility Analysis

Fragility analysis was applied to evaluate the performance of roof sheathing under high wind incorporating the uncertainties in loads and resistance. Following the method described by Masoomi et al. (2018), the wind fragilities for the roof sheathing system can be defined as the conditional probability of exceeding a specific damage state under a given wind speed v

$$Fr(V) = P[DS > ds_i | V = v] \tag{2}$$

The fragility curves were developed using Monte Carlo simulations with 10,000 samples, which led to the convergence of failure probabilities. Fig. 5 summarizes the main steps of the Monte Carlo simulation for the roof sheathing fragility assessment.

Uplift Capacity

For this study, the statistics of the wind-uplift capacity (R) of roof sheathing were obtained for 13 mm × 1.2 m × 2.4 m (1/2 in. × 4 ft × 8 ft) oriented strand board (OSB) fastened to nominal 51 by 102 mm (2 by 4 in.) Southern Yellow Pine (SYP) lumber spaced 24 in. on-center, using 8d common nails [3.33 mm (0.131 in.) diameter, 63.5 mm (2.5 in.) long]. The nail spacing is 15.2 cm (6 in.) along the edge of the panel and 30.5 cm (12 in.) at interior locations. The statistics of uplift capacity were obtained from experimental results by Datin et al. (2011) (Table 3). The uplift capacities of roof panels in the same building are assumed to be partially correlated due to similar environment, material, and construction conditions (He and Hong 2012). For each building sample, the resistance for roof panels is generated from a multivariate lognormal distribution with correlation coefficients equal to 0.4, as suggested by Peng (2013).

Dead Load and Wind Load

The dead load (D) considered in Eq. (1) is the self-weight of the roof sheathing panel. The self-weight of the roof cover, which is assumed to be an asphalt shingle in this study, is negligible compared to the weight of roof sheathing. The dead load is assumed to remain constant in time and is modeled by a normal distribution (Lee and Rosowsky 2005). The statistics of dead load are summarized in Table 3.

In this study, wind loads acting on individual roof panels were calculated based on ASCE 7-16 (ASCE 2016). Wind provisions in ASCE 7-16 focus solely on rectangular buildings, and buildings with nonrectangular footprints are not included. Shao et al. (2018) conducted wind tunnel experiments on L- and T-shaped structures and concluded that wind provisions in the ASCE 7 standard could provide a reasonable estimation of wind pressures acting on complex-shaped roofs. In ASCE 7-16 (ASCE 2016), roof sheathing is modeled as components and cladding (C&C). The wind pressures on C&C of low-rise buildings were determined by the following equation:

$$W = q_h(GC_p - GC_{pi}) \tag{3}$$

where q_h = velocity pressure evaluated at mean roof height; GC_p = external pressure coefficient; and GC_{pi} = internal pressure

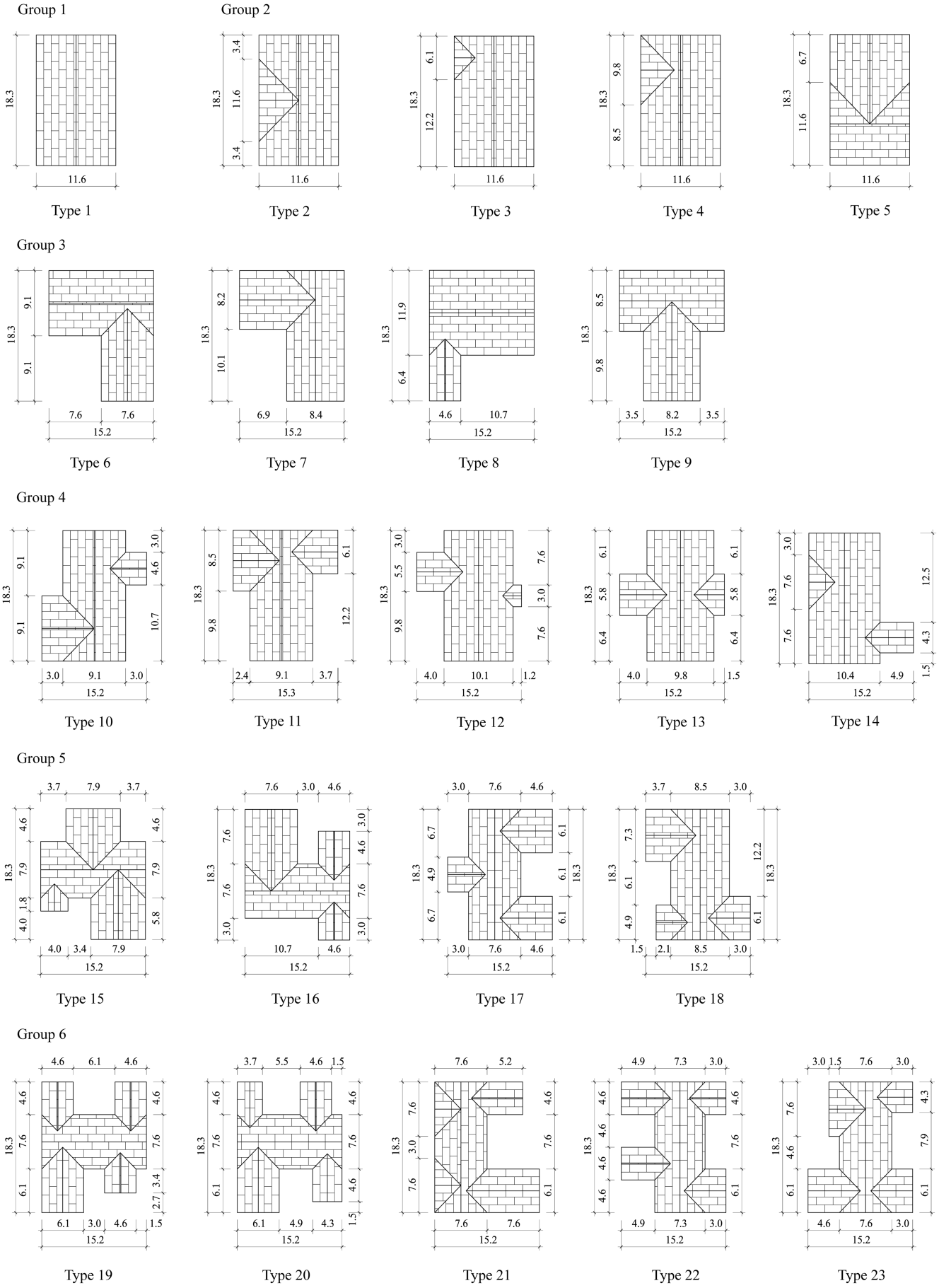

Fig. 1. Dimensions and panel layouts for gable-roofed building models (all dimensions are given in meters).

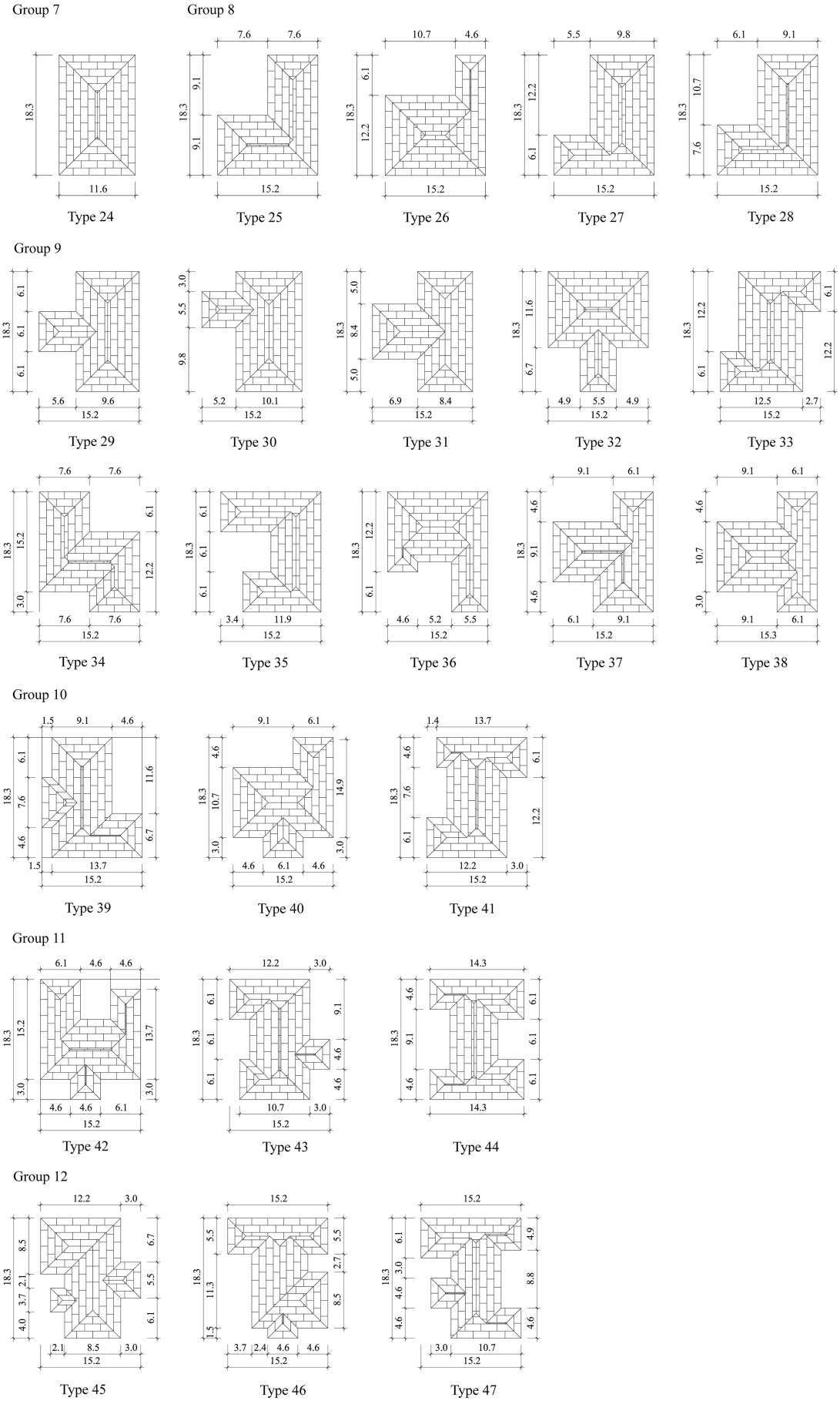

Fig. 2. Dimensions and panel layouts for hip-roofed building models (all dimensions are given in meters).

Table 1. Dimensions and characteristics of building models (Set 1)

Property	Types 1–5	Types 6–23	Type 24	Types 25–47
Plan dimension (m)	11.0 × 17.7	14.6 × 17.7	11.0 × 17.7	14.6 × 17.7
Roof area (m^2)	211.8	209.0 – 210.9	211.8	209.0 – 213.7
Roof type	Gable	Gable	Hip	Hip
No. of stories	1	1	1	1
Wall height (m)	2.4	2.4	2.4	2.4
Roof slope	6:12 (~26.6°)	6:12 (~26.6°)	6:12 (~26.6°)	6:12 (~26.6°)
Roof framing spacing (m)	0.61	0.61	0.61	0.61
Overhang (m)	0.30	0.30	0.30	0.30

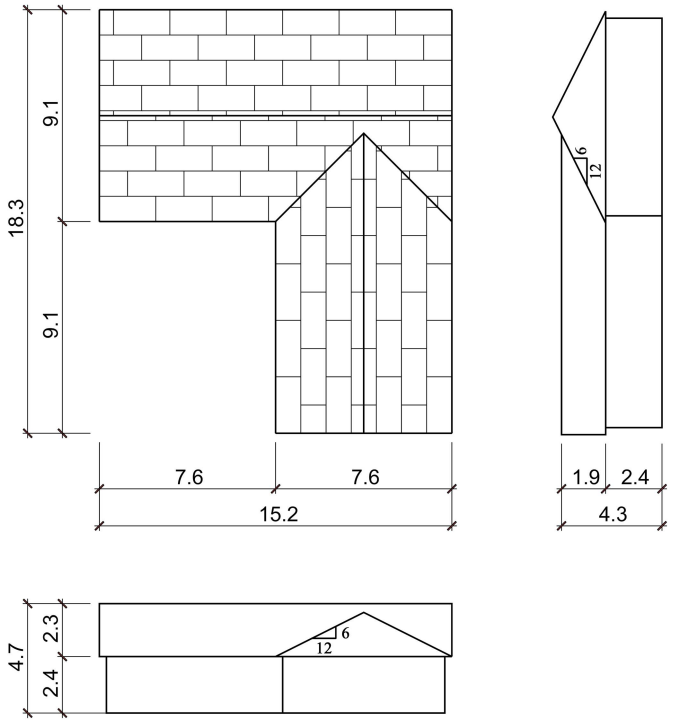

Fig. 3. Dimensions and roof sheathing layout, Structure Type 6 (all dimensions are given in meters).

coefficient. The nominal value of the external pressure coefficient (GC_p) for roof panels was determined using the weighted average method explained by Lee and Rosowsky (2005). The GC_p values for different wind pressure zones are functions of the roof slope given in ASCE 7-16 (ASCE 2016). The velocity pressure, q_h, was determined from ASCE (2016)

$$q_h = 0.00256 K_z K_{zt} K_d V^2 (\text{lb/ft}^2); \quad V \text{ in mi/h} \tag{4}$$

where K_z = velocity pressure exposure coefficient; K_{zt} = topographic factor; K_d = wind directionality factor; and V = 3-s gust speed at 10 m (33 ft) aboveground in open terrain. The velocity pressure exposure coefficient (K_z) is determined based on the mean roof height and the exposure category. For this study, the exposure category is assumed to be Exposure C for open terrain with scattered obstructions. Wind pressures for C&C were determined based on the assumption that wind comes from any possible direction. The wind directionality factor (K_d) was applied to account for the reduced probability of maximum winds coming from any direction and maximum wind pressure occurring for any given wind direction. It is assumed that GC_p follows a normal distribution with the mean-to-nominal value equal to 0.95 and a coefficient of variation equal to 0.12 (Ellingwood and Tekie 1999). The wind zones for GC_p on complex roofs adopted in this paper are illustrated in Fig. 6, which are modified from the wind zones defined for rectangular roofs in ASCE 7-16 (ASCE 2016). The statistics for other wind load parameters used in this study are summarized in Table 3.

In Florida Public Hurricane Loss Model (Gurley et al. 2005), a reduction factor is applied to Eq. (3) to remove the embedded safety factor for wind pressure coefficients provided by ASCE 7. The roof sheathing fragility was reassessed for Building Model Set 1 with the reduction factor to evaluate the potential effect of the reduction factor. The median wind speeds for the fragility curves were increased by 7–9 m/s (15–20 mi/h). The relationships for the fragilities between different groups described in the following sections are still valid, however.

Openings in the building envelope created by failed roof sheathings are likely to change the internal pressure (Stewart et al. 2018; Qin and Stewart 2019; Dev Sarma et al. 2023). The approach proposed by Lee and Rosowsky (2005) was applied in this study to consider this effect. Damage conditions for roof sheathings were first checked with the internal pressure coefficient (GC_{pi}) for an enclosed building. If at least one roof sheathing fails, the internal pressure is recalculated based on a partially enclosed structure. The damage conditions for undamaged roof panels were checked with the updated internal pressure. The positive GC_{pi} values, which result in the worst loading condition for roof sheathing, were used in this study. The statistics for GC_{pi} and other wind load parameters used in this study are summarized in Table 3.

Fragility Curves

Effect of Roof Shape

Gable Roofs

Fig. 7 shows the fragility curves for exceeding DS1 and DS4 of all gable-roofed building models (Types 1–23). The median wind speeds of fragility curves of all gable-roofed buildings are shown in Fig. 8 to illustrate the differences in fragilities between different building models. All building models have very similar standard deviations, and the fragility curves with higher median values have lower failure probability given the same wind speed. As shown in Figs. 7 and 8, the failure probabilities increase with the higher complexity of roof shapes. The rectangular gable roofs (Groups 1–2) experience lower failure probabilities than nonrectangular gable roofs (Groups 3–6), and the difference increases for more severe damage states. For rectangular gable roofs, the simple gable roof (Group 1) is less vulnerable than cross-gable roofs (Group 2), and the difference decreases drastically for more severe damage states. For nonrectangular gable roofs, the structures in the same group show similar performance under high winds, as shown in Fig. 7.

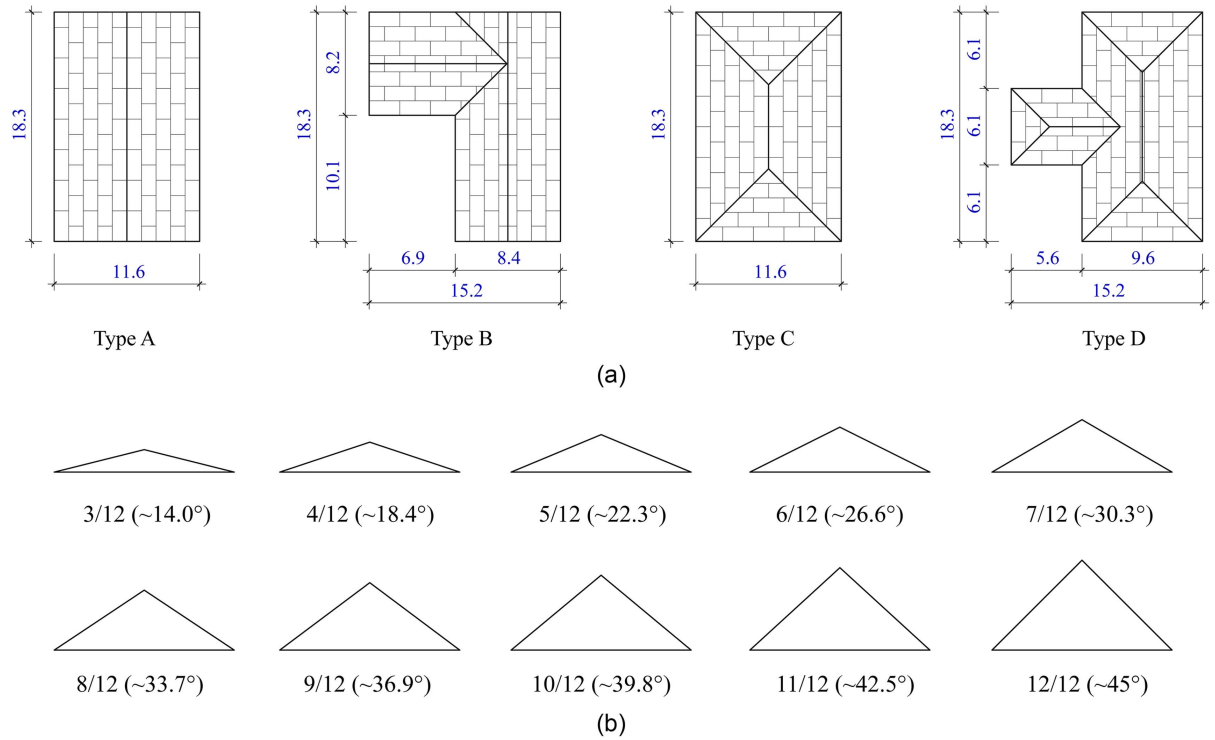

Fig. 4. Characteristics of building models (Set 2): (a) roof configurations and dimensions for baseline building models, with the panel layouts shown for 4:12 pitched roofs; and (b) selected roof pitch (all dimensions are given in meters).

Table 2. Dimensions and characteristics of building models (Set 2)

Property	Type A	Type B	Type C	Type D
Plan dimension (m)	11.0 × 17.7	14.6 × 17.7	11.0 × 17.7	14.6 × 17.7
Roof type	Gable	Gable	Hip	Hip
No. of stories	1	1	1	1
Wall height (m)	2.4	2.4	2.4	2.4
Roof framing spacing (m)	0.61	0.61	0.61	0.61
Overhang (m)	0.30	0.30	0.30	0.30

The probability of no roof sheathing failure for Type 1 (rectangular, one ridgeline) is 13% higher than Type 2 (rectangular, two ridgelines), and 36% higher than Type 21 (complex, five ridgelines) for a wind speed of 63 m/s (142 mi/h). The probability of at least 25% roof sheathing failure for Type 1 is 35% lower than Type 20 (complex, five ridgelines) for a wind speed of 73 m/s (163 mi/h). The aforementioned difference in fragility curves demonstrates that the effect of roof shape on roof sheathing fragility is considerable for gable roofs. The increased roof sheathing failure probabilities with more complex gable roofs can be explained by the distribution of wind pressure on gable roofs. It was observed in wind tunnel tests conducted on rectangular and nonrectangular gable-roofed buildings (Marshall 1975; Gavanski et al. 2013) that peak suction appears along roof ridges, roof edges, and roof corners. A larger portion of the roof panels is located in the high-wind-pressure zones for more complex gable roofs, which results in overall higher wind loads and a higher likelihood of experiencing roof sheathing damage for gable roofs with higher complexity.

Hip Roofs

Fig. 9 shows the fragility curves for hip-roofed buildings (Types 24–47). The median wind speeds for fragility curves for the four damage states are plotted in Fig. 10. The median wind speeds for fragility curves are similar for nonrectangular hip-roofed buildings (Groups 8–12). As shown in Fig. 9, the fragilities show higher variance for more severe damage states (DS3 and DS4). Notable differences in fragilities can be observed between the rectangular hip-roofed building (Type 24) and nonrectangular hip-roofed buildings (Types 25–47) for DS3 and DS4. The probability of at least 25% roof sheathing failure for Type 24 (four roof corners) is 9% lower than Type 37 (five roof corners) for a wind speed of 78 m/s (174 mi/h). In contrast to the gable-roofed buildings, all nonrectangular hip-roofed buildings show similar wind fragilities regardless of the roof complexity. Different effects of roof shape on roof sheathing fragility for gable and hip roofs might be caused by different roof configurations and wind pressure distributions. As shown in Fig. 6, the roof panels near the hip lines and roof edges cover the majority of the roof. The variation of peak negative wind pressures between different wind zones for hip roofs is lower than the gable roofs. When determining the wind loads on roof sheathings for hip roofs, the differentiation between different roof zones is less critical than other building characteristics, like roof height and roof slope, as concluded by Gavanski et al. (2013). In contrast, the differentiation of roof zones was found to be crucial for gable roofs.

Gable versus Hip Roofs

Fig. 11 shows the fragility curves for all gable-roofed buildings are to the left of those for hip-roofed buildings, which indicates that roof sheathing on gable roofs is more likely to be damaged than on hip roofs despite variation in roof shapes. This is consistent with the observations from postdisaster surveys that hip roofs had better performance than gable roofs during hurricanes (NRC 1991; FEMA 1992). As depicted in Fig. 11, the variance of fragilities for gable roofs with different roof configurations is substantially higher than for hip roofs. As summarized in the postdisaster survey of Hurricane Andrew (Crandell et al. 1993), hip roofs experienced significantly

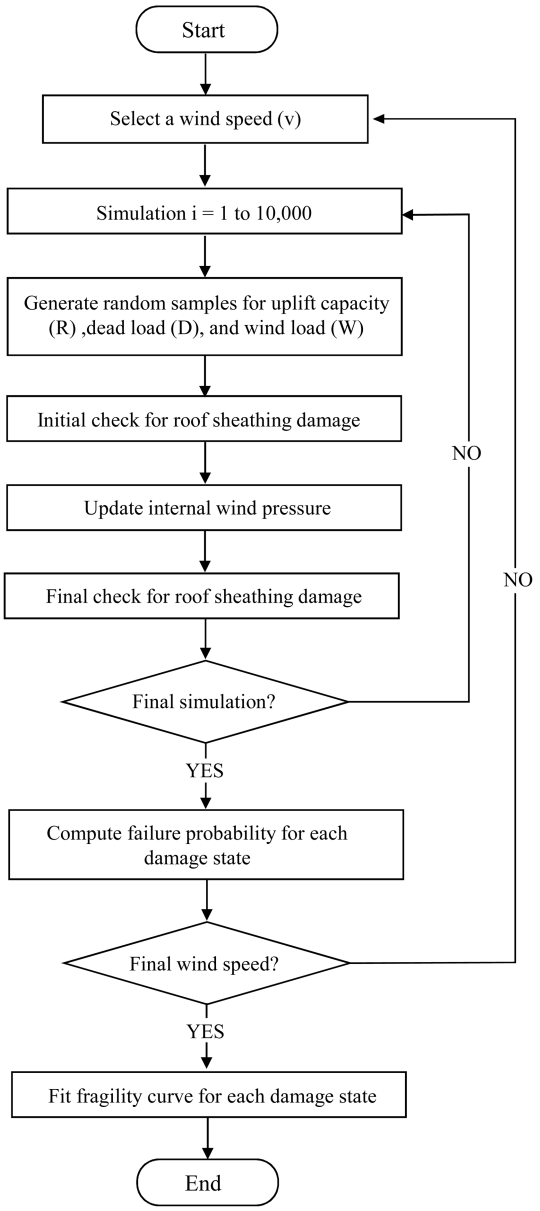

Fig. 5. Simulation procedure for roof sheathing fragility assessment.

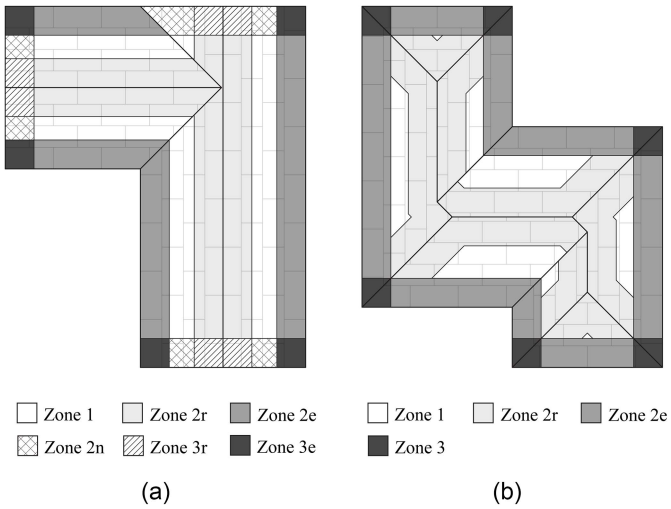

Fig. 6. Wind zones for external wind pressure coefficient (GC_p) for complex roofs: (a) Structure Type 7; and (b) Structure Type 34.

less damage than gable roofs regardless of building shapes, and hip-roofed buildings showed less variance in roof damage ratio compared to gable-roofed buildings. Brown-Giammanco et al. (2018) assessed the roof sheathing damage for residential buildings after Hurricane Harvey. Roof structure damage was mainly observed in neighborhoods experiencing 54 m/s (120 mi/h) to 63 m/s (140 mi/h) gust wind. Gable roofs showed 18% higher roof sheathing damage frequency for roof sheathing than hip roofs. As shown in Fig. 11(a), for a wind speed of 58 m/s (130 mi/h), the probabilities of no roof sheathing failures for a rectangular gable-roofed building (Type 1), an L-shaped gable roof (Type 7), and a gable roof with four ridgelines (Type 15) are 8%, 20%, and 29% lower than the T-shaped hip roof (Type 29). Considering the variation in other building characteristics, the roof sheathing damage probabilities predicted by the fragility analysis show good agreement with the observed damage data.

Statistical Analysis

To evaluate the statistical significance of the results, ANOVA was used to determine whether the fragility parameters (median and standard deviation) of different groups are statistically different at the confidence level of 95%. For gable-roofed building models (Types 1–23), ANOVA analysis shows that rectangular gable-roofed buildings (Groups 1–2) have significantly higher median wind speeds for fragility curves than those with nonrectangular roofs (Groups 3–6). The median wind speeds for Group 3 (two ridgelines) and Group 4 (three ridgelines) have no significant difference in fragility curves for DS1, DS3, and DS4. The median wind speeds for Group 5 (four ridgelines) and Group 6 (five ridgelines) have no significant difference in fragility curves for DS1 and DS2. The median wind speeds differ significantly for fragility curves with other damage states and other groups. As the complexity of roof configuration (i.e., the number of ridgelines) increases, the failure probability of roof sheathing rises significantly.

Table 3. Resistance (R), dead load (D), and wind load statistics

Parameter	Category	Mean	COV	Distribution	Reference
R	8DC6/12	6.20 kPa [129.4 (psf)]	0.12	Lognormal	Datin et al. (2011)
	Closed-cell sprayed polyurethane foam (ccSPF)	7.42 kPa [154.9 (psf)]	0.17	Lognormal	Datin et al. (2011)
D	—	0.17 kPa [3.5 (psf)]	0.1	Normal	Lee and Rosowsky (2005)
K_z	One-story	0.82	0.14	Normal	Lee and Rosowsky (2005)
	Two-story	0.84	0.14	Normal	Lee and Rosowsky (2005)
K_d	Components and cladding	0.89	0.16	Normal	Lee and Rosowsky (2005)
GC_{pi}	Enclosed	0.15	0.33	Normal	Lee and Rosowsky (2005)
	Partially enclosed	0.46	0.33	Normal	Lee and Rosowsky (2005)
K_{zt}	Deterministic (1.0)				Lee and Rosowsky (2005)

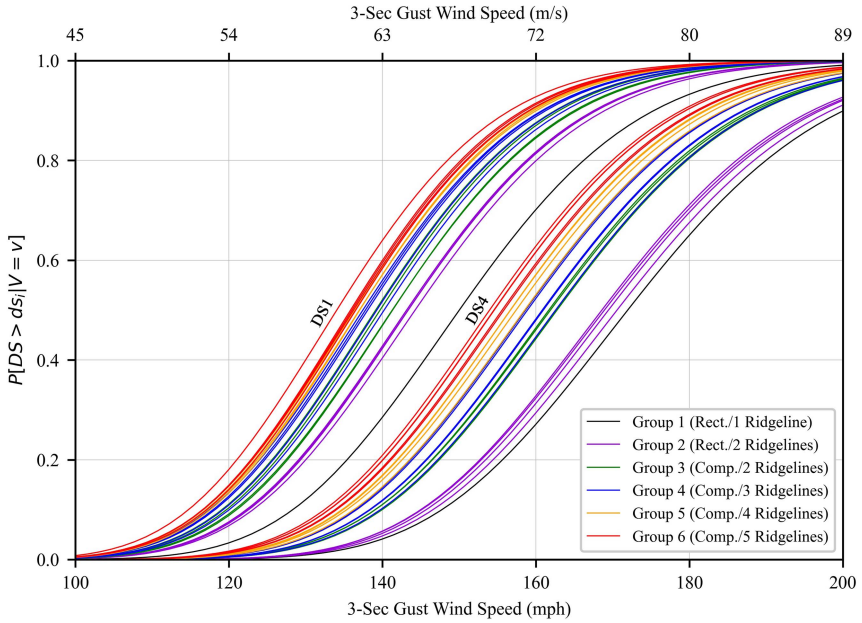

Fig. 7. Fragility curves for gable-roofed buildings (Types 1–23).

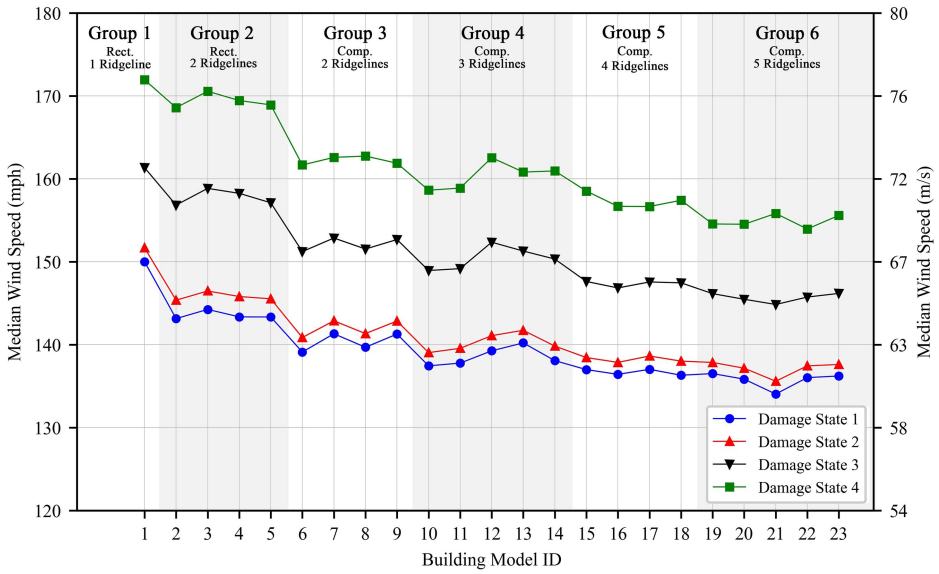

Fig. 8. Median wind speed of fragility curves for gable-roofed buildings (Types 1–23).

For hip-roofed building models (Types 24–47), ANOVA test results show that the median wind speeds for the fragility curves for the rectangular hip roof (Type 24) are significantly higher than or nonrectangular hip roofs (Types 25–47). For nonrectangular hip roofs (Groups 7–11), the fragility parameters do not significantly differ between groups. In summary, rectangular hip roofs have better performance than nonrectangular hip roofs. For nonrectangular hip roofs, the complexity of roof configurations shows a minor effect on the roof sheathing fragility.

Effect of Roof Pitch

Figs. 12 and 13 present the fragility curves and corresponding median wind speeds of gable-roofed buildings (Types A and B) with 10 different roof pitches. For the rectangular gable-roofed building (Type A), as shown in Fig. 12(a), the median wind speeds increase significantly for 5:12 roof pitch compared to those for 3:12 and 4:12 roof pitch. The probability of no roof sheathing failure for Type A of 4:12 roof pitch is 23% lower than 5:12 roof pitch for a wind speed of 63 m/s (142 mi/h). With the increase of roof pitch beyond 5:12, the median wind speeds change moderately. For the complex gable-roofed building (Type B), two notable increments of median wind speeds can be observed when roof pitch exceeds 4:12 and 6:12. The probabilities of more than 25% roof sheathing failure for Structure Type B of 7:12 roof pitch are 35% and 10% higher than for 4:12 and 5:12 roof pitches, respectively, for a wind speed of 72 m/s (161 mi/h). For roofs steeper than 6:12, similar to Type A, roof pitch shows a moderate effect on roof sheathing fragilities.

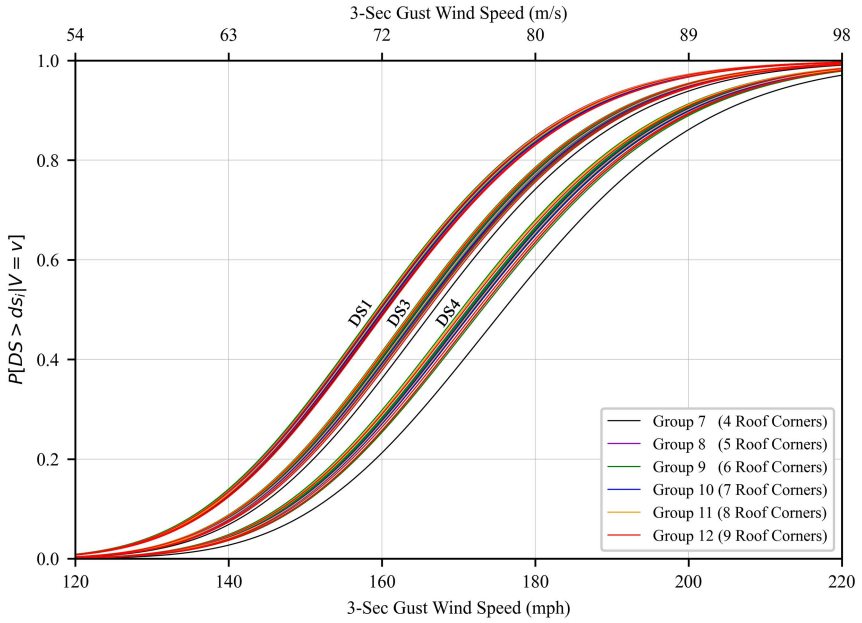

Fig. 9. Fragility curves for hip-roofed buildings (Types 24–47).

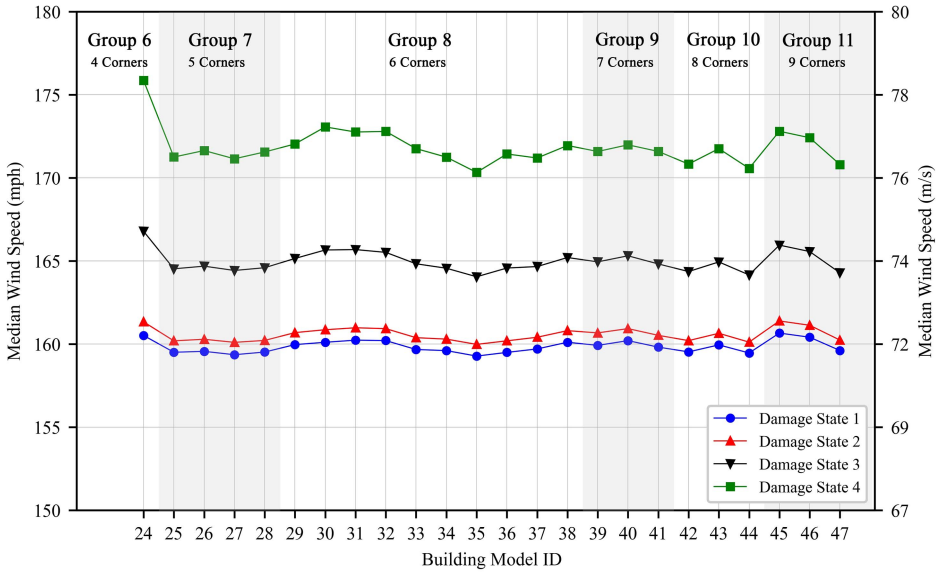

Fig. 10. Median wind speed of fragility curves for hip-roofed buildings (Types 24–47).

For hip-roofed buildings, similar trends between roof pitch and roof sheathing fragilities for Structure Types C and D can be found in Figs. 14 and 15. For frequently used hip-roofed pitches (3:12–6:12), the variation of roof pitch influences roof sheathing fragilities moderately. The probability of no roof sheathing failure for Type D with 5:12 roof pitch is 8% higher than that for 3:12 roof pitch for a wind speed of 71 m/s (158 mi/h). As shown in Fig. 14, for Types C and D, the median wind speeds reach the maximum value for 7:12 roof pitch and drop rapidly for higher pitch angles. Generally, roof pitch shows more substantial effects on the fragilities of the complex hip-roofed building (Type D) than rectangular hip-roofed building (Type C) for roof pitches smaller 7:12.

In summary, the effect of roof pitch on roof sheathing fragilities is substantial for gable roofs with a roof pitch smaller than 7:12 and hip roofs with a roof pitch larger than 6:12. For gable roofs with roof pitches smaller than 7:12, roof pitch shows a stronger effect on roof sheathing fragilities for complex roofs than those for simple roofs. For hip roofs, the effect of roof pitch sheathing fragilities is similar for simple and complex roofs.

Comparison with Other Characteristics

Fragility analysis was applied to selected building models with modified building properties to assess the importance of roof type and roof pitch relative to other critical building and structural characteristics. Fragility curves for Type 7 (L-shaped gable roof) and Type 29 (T-shaped hip roof) with different resistance types, number of stories, and overhang conditions are shown in Figs. 16 and 17.

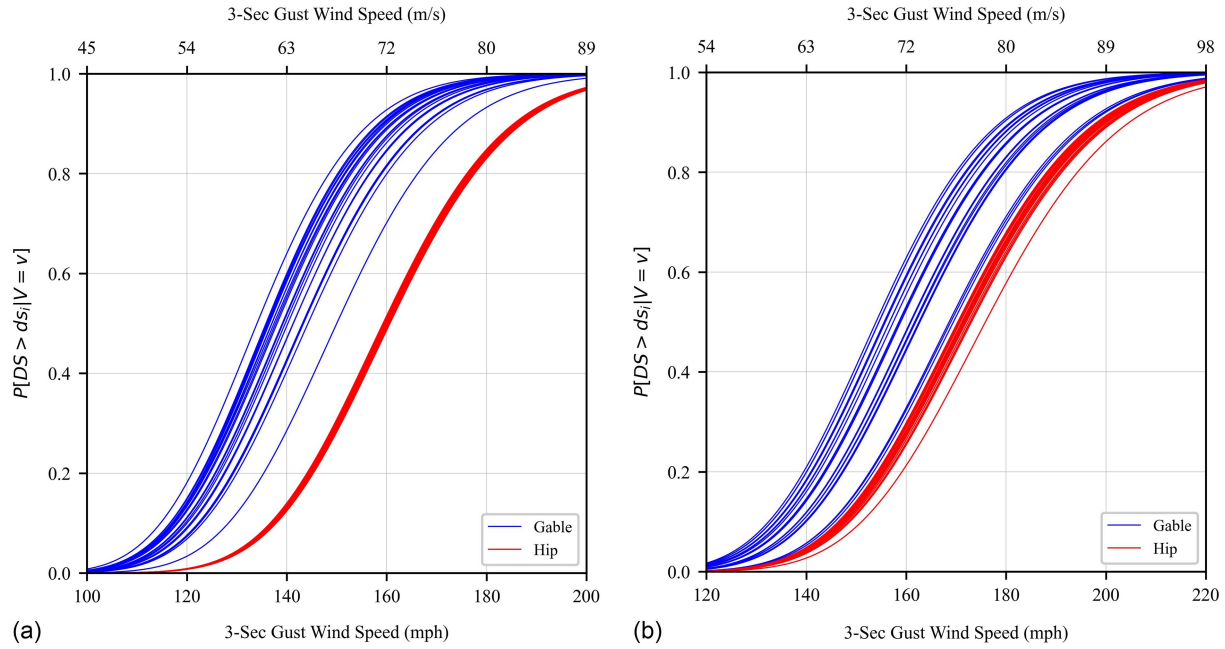

Fig. 11. Fragility curves for all buildings in Building Model Set 1: (a) DS1; and (b) DS4.

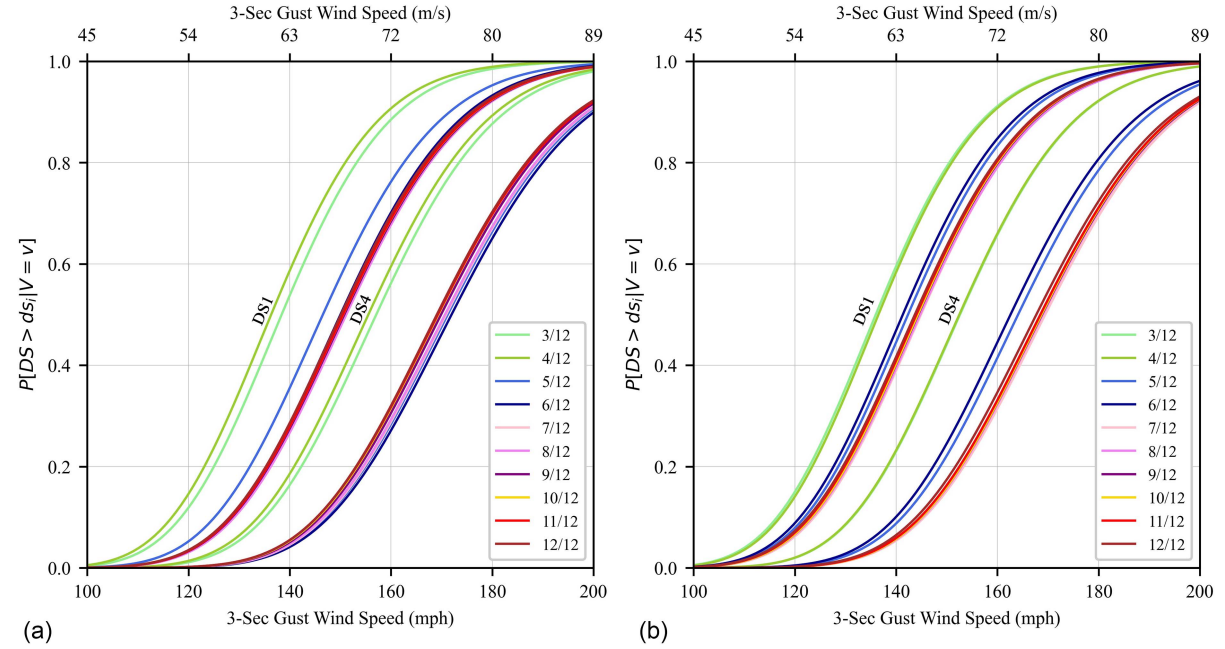

Fig. 12. Fragility curves for gable-roofed buildings with different roof pitches: (a) Structure Type A; and (b) Structure Type B.

To evaluate the effect of resistance on roof sheathing fragilities, the fragility curves were developed for structures with closed-cell sprayed polyurethane foam (ccSPF) retrofitted panels (Table 3). Fragility curves for Type 1 (simple rectangular gable roof) and Type 24 (rectangular hip roof) are used to demonstrate the effect of roof configurations. Fig. 16 suggests the effects of roof shape and roof pitch are as critical as the uplift capacity for gable roofs. The impact of roof overhang and the number of stories on roof sheathing fragilities is moderate compared to other characteristics. For the hip roofs, the roof shape and roof pitch show minor effects on the fragilities compared to other properties, as shown in Fig. 17.

Regional Loss Consequences

Across the United States, single-family housing inventories have a wide range of roof shapes. Yet, existing regional hurricane loss models only allow for three roof shape configurations for single-family housing units: simple gable, simple hip, and flat roofs (Deierlein et al. 2020; Nofal et al. 2021; FEMA 2021; Wang et al. 2020). Due to the higher fragilities of more complex roof shapes, as exhibited previously, the exclusion of complex roof shapes in regional hurricane loss modeling may lead to an underestimation of regional losses. This section evaluates the impacts on loss estimates when

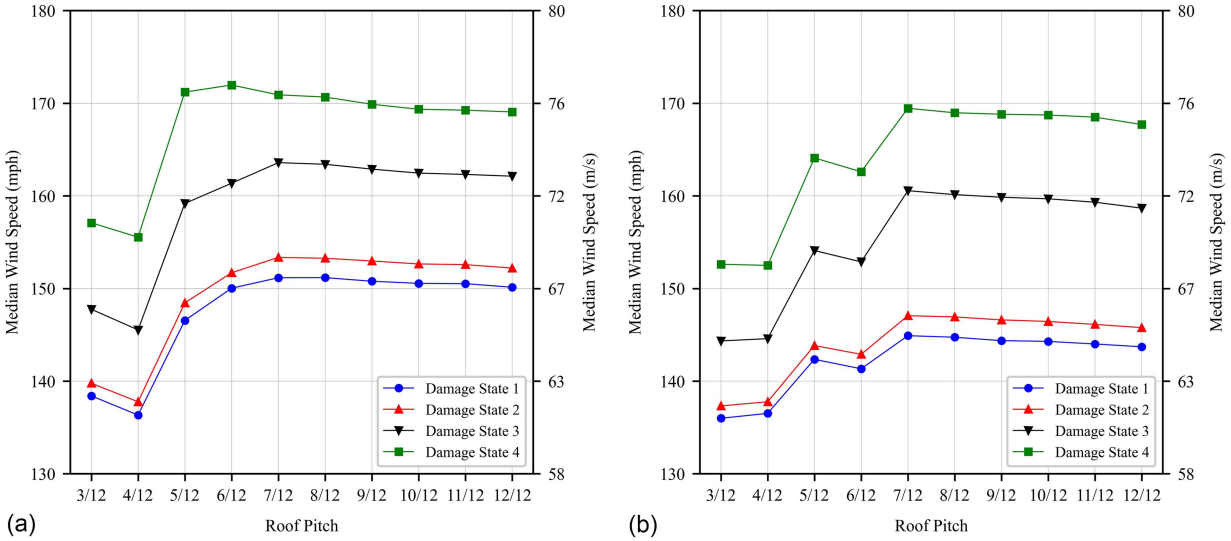

Fig. 13. Median wind speed of fragility curves for gable-roofed buildings: (a) Structure Type A; and (b) Structure Type B.

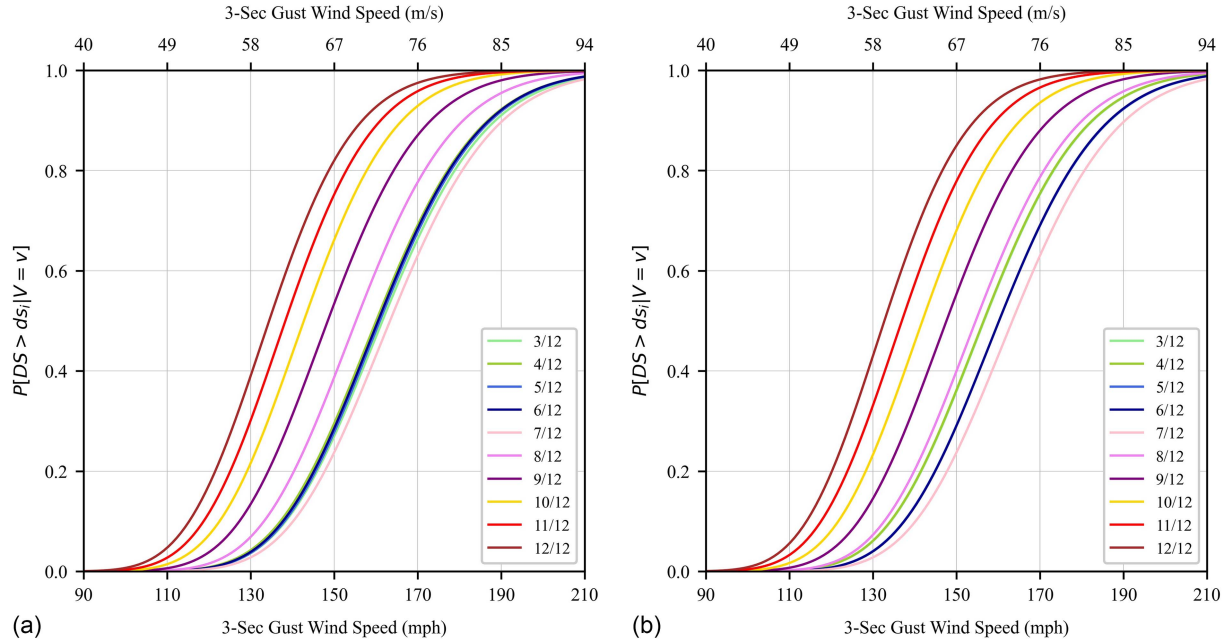

Fig. 14. Fragility curves for hip-roofed buildings with different roof pitches (DS1): (a) Structure Type C; and (b) Structure Type D.

complex roof shapes are included in regional hurricane loss models for single-family structures, using New Hanover County, North Carolina, as a case study. Unlike the fragility analysis, the regional loss analysis includes the extent to which complex roof shapes exist in New Hanover County, as well as the likelihood of experiencing damaging wind speeds, both of which help determine the extent to which simplifying the representation of roof shapes introduces loss estimate errors.

Regional Loss Modeling Methods

The component-based loss model is a simulation combining hazard, inventory, and damage modules to compute a probability distribution of losses for each group of buildings (defined by location and building type) and specified hurricanes in the study area. We developed the model used in this study to estimate wind damage and direct loss based in part on an early version of the Florida Public Hurricane Loss Model as described in Gurley et al. (2005) and Pinelli et al. (2004, 2008). It was previously used in Peng (2013), Peng et al. (2014), Gao et al. (2016), and Wang et al. (2020).

New Hanover County, which includes the city of Wilmington, is located on the southeastern coast of North Carolina and includes approximately 72,425 single-family housing units (Zillow 2020). The county was divided into 67 zones, where each zone corresponded to a 2010 census tract, except for the census tracts along the coast, which were divided into three smaller zones. Building types were defined to represent all combinations of the number of stories (one or two), garage (yes or no), and roof shape (two roof shapes

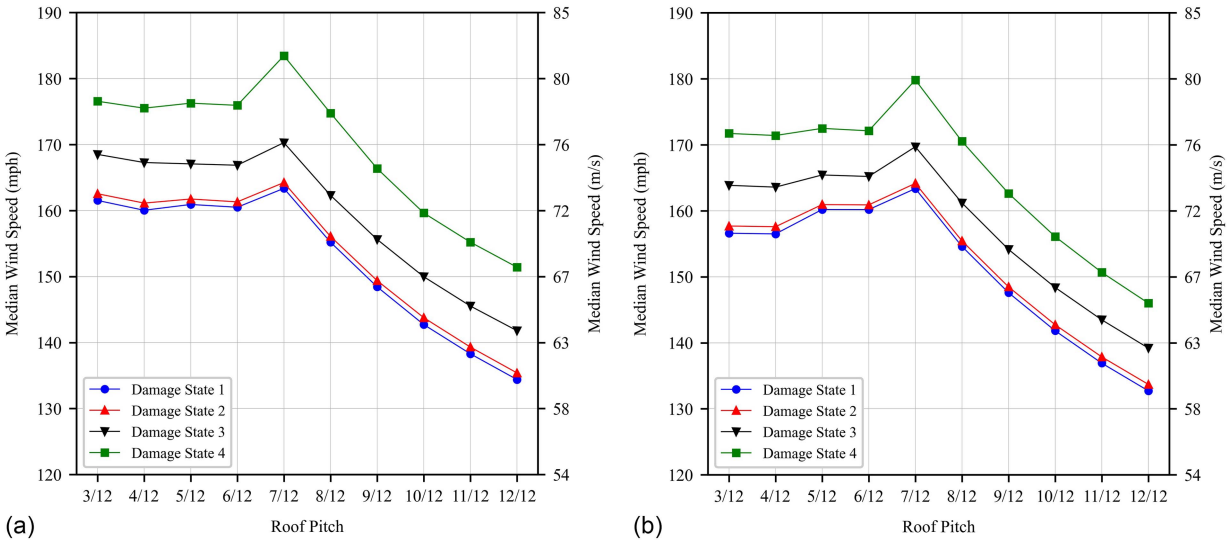

Fig. 15. Median wind speed of fragility curves for hip-roofed buildings: (a) Structure Type C; and (b) Structure Type D.

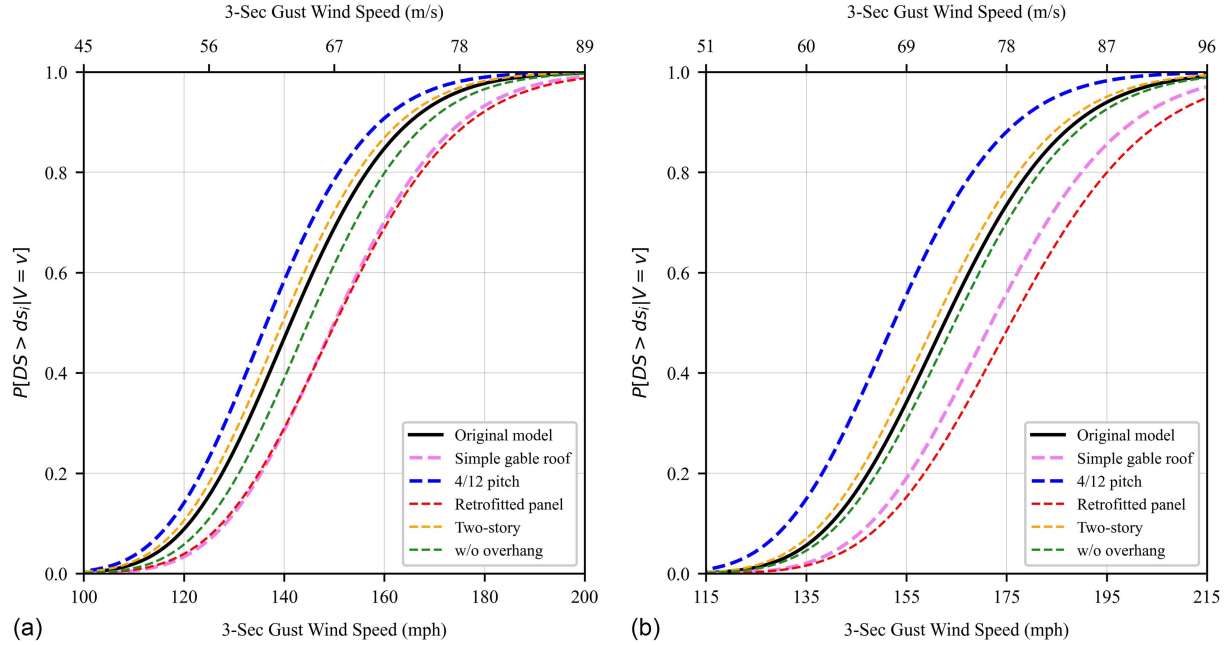

Fig. 16. Fragility curves for Type 7 with different building characteristics: (a) DS1; and (b) DS4.

or five roof shapes, depending on the analysis). Each building is defined as a collection of components represented in the damage and loss model (e.g., roof cover, roof sheathing, roof-to-wall connection, windows, and openings). Each component in turn is made of many component units (e.g., a single window or section of roof covering).

The definition of the building inventory was the same as that was used in Peng (2013) and Peng et al. (2014), with two exceptions. First, the number of houses in each zone was based on Zillow's ZTRAX database (Zillow 2020), rather than the US Census. Second, in addition to the base analysis that assumes all roofs are simple gable or simple hip, we conducted a second analysis in which each roof was assigned one of five roof shapes (simple gable, simple cross gable, complex cross gable, simple hip, cross hip) (Fig. 18). The roof shapes in New Hanover County are estimated to be 22% simple gable, 22% simple cross gable, 36% complex cross gable, 5% simple hip, and 15% cross hip. The distribution of the roof shapes in New Hanover was identified by sampling 10% of the single-family houses in each zone and retrieving the corresponding satellite images from Google Maps. The sampled satellite images were then manually classified into the five roof shape categories. Of the 7,242 sampled satellite images, 19% did not have a visible roof image (largely due to tree cover) and were thus classified as not available. Even for the complex, nonrectangular roof shapes, the same rectangular building footprints, walls, and openings were used so the only difference between the two runs was the roof shapes. A future study could investigate the regional loss effects when incorporating both nonrectangular roof shapes and associated nonrectangular building footprints, walls, and openings.

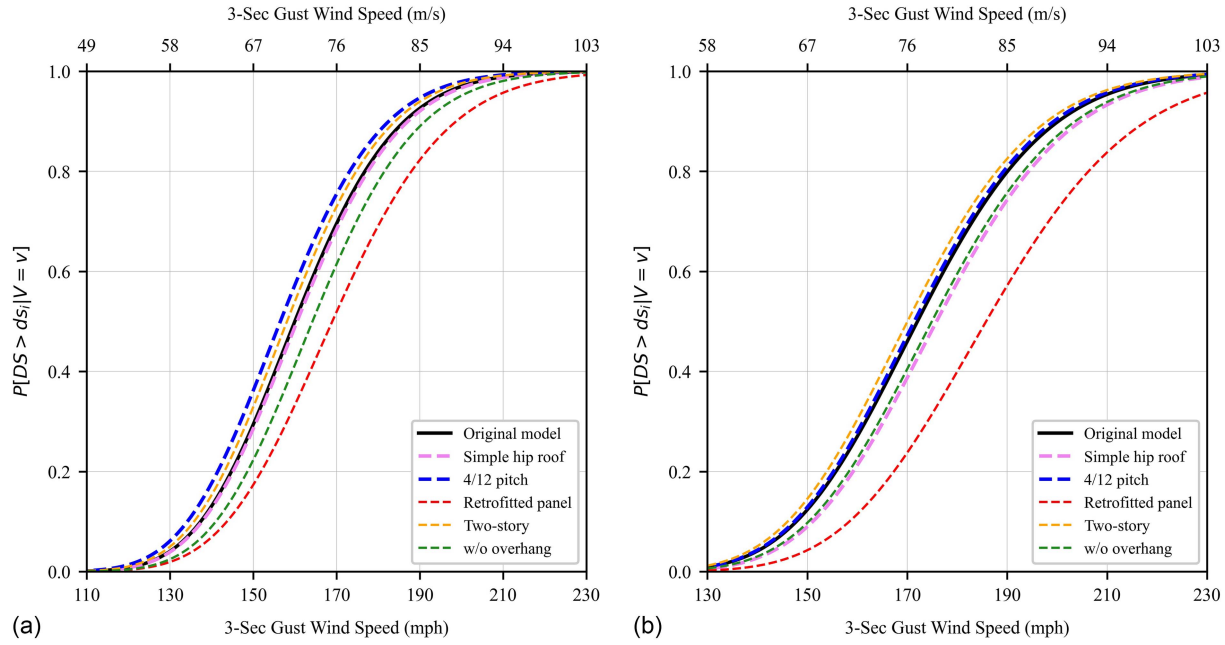

Fig. 17. Fragility curves for Type 29 with different building characteristics: (a) DS1; and (b) DS4.

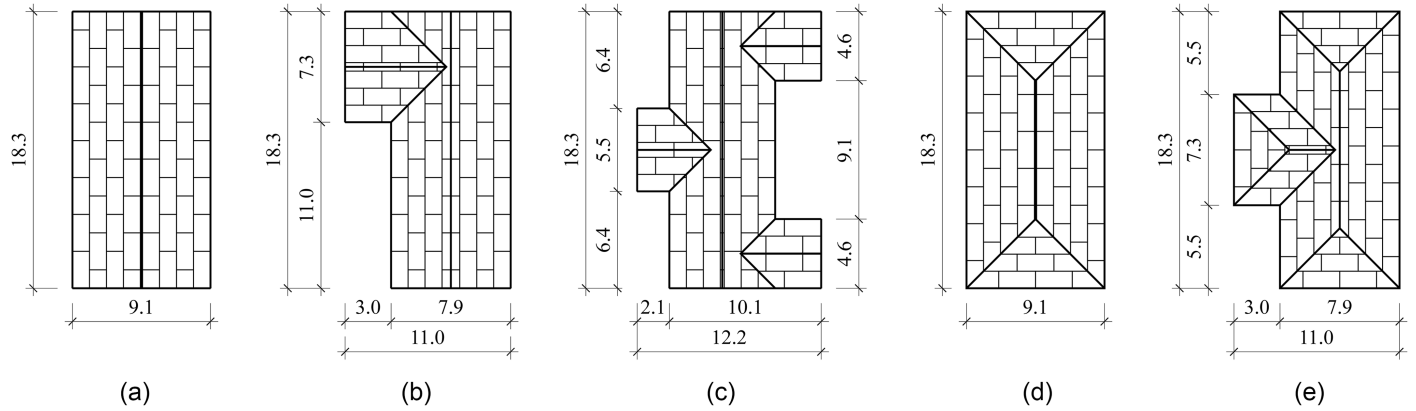

Fig. 18. Dimensions and panel layouts for building models used for regional loss model: (a) simple gable; (b) simple cross gable; (c) complex cross gable; (d) simple hip; and (e) cross hip (all dimensions are given in meters).

The hazard was represented using the set of 97 hurricane scenarios developed in Apivatanagul et al. (2011), each with a corresponding annual probability and map of 3-s peak gust wind speed throughout the area.

Effects of Complex Roof Inventories on Regional Loss

Results suggest a substantial underestimation of hurricane losses when complex roof shapes for single-family houses are not accounted for in regional loss modeling. If all roofs are assumed to be rectangular hip or rectangular gable in New Hanover County, the expected annual roof sheathing losses would be $2.7 million. However, if a complex roof inventory with five different roof shapes was included in the model, as would be more realistic, the resulting expected annual roof sheathing losses would be $3.8 million. This results in a $1.1 million (44.4%) increase in roof sheathing losses. The reported roof sheathing losses only represent the direct cost for roof sheathing replacement. They do not include the consequential damages to interior components or related internal pressure effects when roof sheathing damage occurs.

Additionally, the differences between the loss estimates for complex and simple roof inventories vary as hurricane wind speeds increase, suggesting that the importance of including complex roof shapes may vary for different ranges of wind speeds. The percent difference between estimated losses with complex roof inventories versus simple roof inventories increases to 56% as hurricane intensity increases up to approximately 49.7 m/s (111.2 mi/h). At this point, the difference then decreases to approximately 20% for the largest simulated hurricane [66.7 m/s (149.1 mi/h)] (Fig. 19). This suggests the incorporation of roof shape in regional loss modeling is an important aspect when modeling roof sheathing damages for all hurricane events.

Roof shape affects not only damage to the roof sheathing but also the roof cover. The expected annual roof cover losses are an order of magnitude larger than roof sheathing at $11.6 million and $15.2 million for simple and complex roof inventories, respectively. The higher loss estimates account for the fact that roof cover damage occurs at lower wind speeds. Additionally, the percent difference between the estimated losses for complex and simple roof inventories follows a similar pattern as roof sheathing, where the

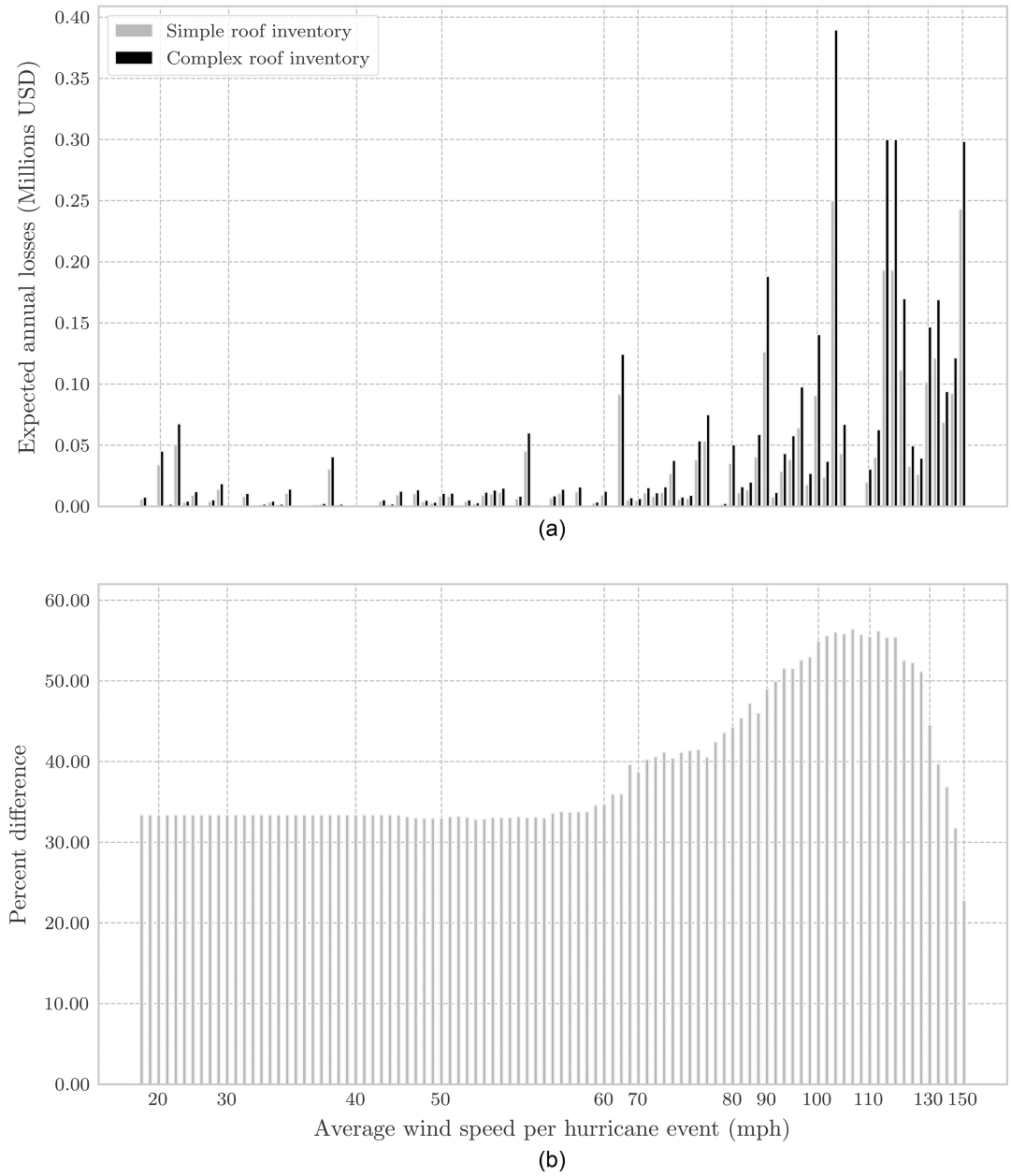

Fig. 19. Expected roof sheathing losses. Each bar represents one hurricane event. (a) Expected annual roof sheathing losses for the 97 simulated hurricanes in New Hanover County. Each hurricane event is represented as its average peak 3-s wind gust speed across the county. (b) Percent difference in the expected annual roof sheathing losses between a complex roof inventory and simple roof inventory for the 97 simulated hurricane events in New Hanover County.

difference increases to 53% as wind speeds increase up to approximately 37.1 m/s (83.0 mi/h), at which point the difference then decreases rapidly, again highlighting the importance of including realistic roof shapes in a regional loss model.

Limitations

This study aims to provide an evaluation of the effects of roof shape and roof pitch on roof sheathing fragility using the analysis methods adopted by current wind vulnerability models, including the FEMA HAZUS-MH model (Vickery et al. 2006) and the FPHLM model (Hamid 2019), and previous research on fragility analysis for nonrectangular buildings (Amini and van de Lindt 2014; Masoomi et al. 2018). Due to the lack of data on wind pressures on complex roofs, key assumptions were made when conducting the fragility analysis for roof sheathing.

First, the wind pressures applied on roof sheathing were calculated using the code-based method. Wind pressures were determined based on the maximum wind pressure considering all possible wind directions instead of a specific wind direction because the wind pressure data for directional cases are unavailable for nonrectangular buildings. As shown in Eqs. (3) and (4), a wind directionality factor (K_d) is applied to account for the reduced probabilities of maximum winds coming from any given direction and the maximum pressure coefficient occurring for any given wind direction (ASCE 2016). As discussed by Lee and Rosowsky (2005), the wind directionality factor is conservative, and the actual wind pressures should be lower than those used in this study.

Second, the change in internal wind pressure due to the damage of openings (e.g., windows, doors) is not considered in the fragility analysis. If the increase of internal wind pressure due to the damage of openings were considered, the failure probabilities for roof sheathing would be higher than those shown in this paper.

Third, the external wind pressure coefficients (GC_p) provided in ASCE 7-16 (ASCE 2016) are determined based on the roof pitch. For ease of use, the roof pitches are classified into three groups (7°–20°, 20°–27°, and 27°–45°), and the GC_p values for roof pitches within the same group are assumed to be the same, except for hip roofs with roof pitches larger than 27°. As a result, the fragility curves in Figs. 12 and 14 may have a larger variance for roof pitches within the same group and a smaller variance between different groups when using more accurate wind pressure data.

Last, the regional loss model conducted for New Hanover County only accounted for the effects of a more complex roof inventory, yet did not analyze the effects of a nonrectangular building footprint. Future work could develop a set of nonrectangular building geometries to better reflect a more realistic and diverse housing inventory.

Conclusions

The inclusion of complex roof geometries in building- and regional-level hurricane loss analyses is important to avoid underestimation of building damages. For example, by including nonrectangular roof geometries in a regional hurricane loss model for New Hanover County, North Carolina, annual expected roof sheathing losses were estimated to be 44% higher ($1.1 million) as compared to a building inventory with only rectangular roof geometries. When studying the effects of two critical parameters for roof sheathing fragility, roof shape, and roof pitch, the fragility analysis indicates that roof shape has a more significant effect on roof sheathing fragility for gable roofs than for hip roofs. For gable roofs with more complex configurations, roof sheathing experiences higher failure probabilities and shows a larger variance in fragilities. On the contrary, wind fragilities for hip roofs show minimal differences for different roof shapes. Among all building models, despite variations in roof shapes, gable-roofed buildings show higher fragilities than hip-roofed buildings. For gable and hip roofs, a larger variance in roof sheathing fragility is observed for more severe damage states.

Results for building models with different roof pitches show that roof pitch also influences roof sheathing fragility considerably. For roof pitches smaller than 7:12, the failure probabilities of roof sheathing panels in gable roofs decrease rapidly with the increase of roof pitch. For hip roofs, roof pitch has a moderate effect on roof sheathing fragility when the roof pitch is smaller than 7:12. When the roof pitch exceeds 6:12, the failure probability of roof sheathing in hip roofs increases drastically when the roof pitch rises.

When modeling roofs for a wind vulnerability assessment of roof sheathing in single-family homes, it is reasonable to neglect the roof shape and pitch variation for intermediate sloped (3:12–6:12) hip roofs. However, for gable-roofed buildings, modeling complex roofs using simple rectangular roofs, as adopted in current wind vulnerability models, may underestimate the failure probability of roof sheathing and the associated economic loss. The variation of roof pitch for gable roofs should also be considered in the roof models. The enriched building inventories, which include realistic roof type and roof pitch data extracted from remote sensing data, have the potential to improve roof damage estimates for both individual building- and regional-level hurricane loss analyses.

Data Availability Statement

Some or all data, models, or code that support the findings of this study are available from the corresponding author upon reasonable request. Some or all data, models, or code used during the study were provided by a third party. Direct requests for these materials may be made to the provider as indicated in the Acknowledgments.

Acknowledgments

We are grateful for financial support from the National Science Foundation (NSF) (Awards 1830511 and 2209190). Some of the building metadata used in this study were provided by Zillow through the Zillow Transaction and Assessment Dataset (ZTRAX). More information on accessing the data can be found at http://www.zillow.com/ztrax. The results and opinions are those of the authors and do not reflect the position of NSF or the Zillow Group.

Notation

The following symbols are used in this paper:

D = dead load;
GC_p = external pressure coefficient;
GC_{pi} = internal pressure coefficient;
K_d = wind directionality factor;
K_z = velocity pressure exposure coefficient;
K_{zt} = topographic factor;
q_h = velocity pressure evaluated at mean roof height;
R = uplift capacity of roof sheathing;
V = 3-s gust speed at 10 m (33 ft) aboveground in open terrain; and
W = uplift wind load acting on the roof sheathing.

References

Amini, M. O., and J. W. van de Lindt. 2014. "Quantitative insight into rational tornado design wind speeds for residential wood-frame structures using fragility approach." *J. Struct. Eng.* 140 (7): 04014033. https://doi.org/10.1061/(ASCE)ST.1943-541X.0000914.

Apivatanagul, P., R. Davidson, B. Blanton, and L. Nozick. 2011. "Long-term regional hurricane hazard analysis for wind and storm surge." *Coastal Eng.* 58 (6): 499–509. https://doi.org/10.1016/j.coastaleng.2011.01.015.

ASCE. 2010. *Minimum design loads and associated criteria for buildings and other structures*. ASCE/SEI 7-10. Reston, VA: ASCE.

ASCE. 2016. *Minimum design loads and associated criteria for buildings and other structures*. ASCE/SEI 7-16. Reston, VA: ASCE.

Brown-Giammanco, T. M., I. M. Giammanco, and H. Pogorzelski. 2018. *Hurricane Harvey wind damage investigation*. Richburg, SC: Insurance Institute for Business and Home Safety.

Crandell, J. H., M. Nowak, E. M. Laatsch, A. van Overeem, C. Barbour, R. Dewey, H. Reigel, and H. Angleton. 1993. *Assessment of damage to single-family homes caused by Hurricanes Andrew and Iniki*. Upper Marlboro, MD: US Dept. of Housing and Urban Development's Office of Policy Development and Research.

Datin, P. L., D. O. Prevatt, and W. Pang. 2011. "Wind-uplift capacity of residential wood roof-sheathing panels retrofitted with insulating foam adhesive." *J. Archit. Eng.* 17 (4): 144–154. https://doi.org/10.1061/(ASCE)AE.1943-5568.0000034.

Deierlein, G. G., F. McKenna, A. Zsarnóczay, T. Kijewski-Correa, A. Kareem, W. Elhaddad, L. Lowes, M. J. Schoettler, and S. Govindjee. 2020. "A cloud-enabled application framework for simulating regional-scale impacts of natural hazards on the built environment." *Front. Built Environ.* 6 (Nov): 558706. https://doi.org/10.3389/fbuil.2020.558706.

Dev Sarma, H., I. Zisis, and M. Matus. 2023. "Effect of roof shape on wind vulnerability of roof sheathing panels." *Struct. Saf.* 100 (Jan): 102283. https://doi.org/10.1016/j.strusafe.2022.102283.

Ellingwood, B. R., D. V. Rosowsky, Y. Li, and J. H. Kim. 2004. "Fragility assessment of light-frame wood construction subjected to wind and earthquake hazards." *J. Struct. Eng.* 130 (12): 1921–1930. https://doi.org/10.1061/(ASCE)0733-9445(2004)130:12(1921).

Ellingwood, B. R., and P. B. Tekie. 1999. "Wind load statistics for probability-based structural design." *J. Struct. Eng.* 125 (4): 453–463. https://doi.org/10.1061/(ASCE)0733-9445(1999)125:4(453).

El Merabet, Y., C. Meurie, Y. Ruichek, A. Sbihi, and R. Touahni. 2015. "Building roof segmentation from aerial images using a line-and region-based watershed segmentation technique." *Sensors* 15 (2): 3172–3203. https://doi.org/10.3390/s150203172.

FEMA. 1992. *Building performance: Hurricane Andrew in Florida*. Washington, DC: FEMA.

FEMA. 2021. *Hazus–MH 4.2: Hurricane model technical manual*. Washington, DC: FEMA.

Gao, Y., L. Nozick, J. Kruse, and R. Davidson. 2016. "Modeling competition in a market for natural catastrophe insurance." *J. Insur. Issues* 39 (1): 38–68.

Gavanski, E., B. Kordi, G. A. Kopp, and P. J. Vickery. 2013. "Wind loads on roof sheathing of houses." *J. Wind Eng. Ind. Aerodyn.* 114 (Mar): 106–121. https://doi.org/10.1016/j.jweia.2012.12.011.

Gurley, K., J. P. Pinelli, C. Subramanian, A. Cope, L. Zhang, J. Murphree, A. Artiles, P. Misra, S. Culati, and E. Simiu. 2005. *Florida public hurricane loss projection model engineering team final report*. Miami: Florida International Univ.

Hamid, S. S. 2019. *Florida public hurricane loss model, version 8.1*. Florida Commission on Hurricane Loss Projection Methodology. Miami: Florida International Univ.

He, W. X., and H. P. Hong. 2012. "Probabilistic characterization of roof panel uplift capacity under wind loading." *Can. J. Civ. Eng.* 39 (12): 1285–1296. https://doi.org/10.1139/l2012-114.

Kashani, A. G., A. J. Graettinger, and T. Dao. 2016. "Lidar-based methodology to evaluate fragility models for tornado-induced roof damage." *Nat. Hazard. Rev.* 17 (3): 04016006. https://doi.org/10.1061/(ASCE)NH.1527-6996.0000224.

Lee, K. H., and D. V. Rosowsky. 2005. "Fragility assessment for roof sheathing failure in high wind regions." *Eng. Struct.* 27 (6): 857–868. https://doi.org/10.1016/j.engstruct.2004.12.017.

Li, Y. 2005. "Fragility methodology for performance-based engineering of wood-frame residential construction." Ph.D. thesis, Dept. of Civil and Environmental Engineering, Georgia Institute of Technology.

Liu, H., and P. J. Saathoff. 1981. "Building internal pressure: Sudden change." *J. Eng. Mech. Div.* 107 (2): 309–321. https://doi.org/10.1061/JMCEA3.0002707.

Marshall, R. D. 1975. "A study of wind pressures on a single-family dwelling in model and full scale." *J. Wind Eng. Ind. Aerodyn.* 1 (Jan): 177–199. https://doi.org/10.1016/0167-6105(75)90013-6.

Masoomi, H., M. R. Ameri, and J. W. van de Lindt. 2018. "Wind performance enhancement strategies for residential wood-frame buildings." *J. Perform. Constr. Facil.* 32 (3): 04018024. https://doi.org/10.1061/(ASCE)CF.1943-5509.0001172.

Nofal, O. M., J. W. van De Lindt, T. Q. Do, G. Yan, S. Hamideh, D. T. Cox, and J. C. Dietrich. 2021. "Methodology for regional multihazard hurricane damage and risk assessment." *J. Struct. Eng.* 147 (11): 04021185. https://doi.org/10.1061/(ASCE)ST.1943-541X.0003144.

NRC (National Research Council). 1991. *Hurricane Elena, Gulf Coast: August 29-September 2, 1985*. Washington, DC: National Academies Press.

Peng, J. 2013. "Modeling natural disaster risk management: Integrating the roles of insurance and retrofit and multiple stakeholder perspectives." Ph.D. dissertation, Dept. of Civil and Environmental Engineering, Univ. of Delaware.

Peng, J., X. G. Shan, Y. Gao, Y. Kesete, R. A. Davidson, L. K. Nozick, and J. Kruse. 2014. "Modeling the integrated roles of insurance and retrofit in managing natural disaster risk: A multi-stakeholder perspective." *Nat. Hazards* 74 (2): 1043–1068. https://doi.org/10.1007/s11069-014-1231-3.

Pinelli, J.-P., K. Gurley, C. Subramanian, S. Hamid, and G. Pita. 2008. "Validation of a probabilistic model for hurricane insurance loss projections in Florida." *Reliab. Eng. Syst. Saf.* 93 (12): 1896–1905. https://doi.org/10.1016/j.ress.2008.03.017.

Pinelli, J.-P., G. Pita, K. Gurley, B. Torkian, S. Hamid, and C. Subramanian. 2011. "Damage characterization: Application to Florida public hurricane loss model." *Nat. Hazard. Rev.* 12 (4): 190–195. https://doi.org/10.1061/(ASCE)NH.1527-6996.0000051.

Pinelli, J.-P., E. Simiu, K. Gurley, C. Subramanian, L. Zhang, A. Cope, J. J. Filliben, and S. Hamid. 2004. "Hurricane damage prediction model for residential structures." *J. Struct. Eng.* 130 (11): 1685–1691. https://doi.org/10.1061/(ASCE)0733-9445(2004)130:11(1685).

Qin, H., and M. G. Stewart. 2019. "System fragility analysis of roof cladding and trusses for Australian contemporary housing subjected to wind uplift." *Struct. Saf.* 79 (Jul): 80–93. https://doi.org/10.1016/j.strusafe.2019.03.005.

Shao, S., T. Stathopoulos, Q. Yang, and Y. Tian. 2018. "Wind pressures on 4:12-sloped hip roofs of L- and T-shaped low-rise buildings." *J. Struct. Eng.* 144 (7): 04018088. https://doi.org/10.1061/(ASCE)ST.1943-541X.0002077.

Sparks, P. R., S. D. Schiff, and T. A. Reinhold. 1994. "Wind damage to envelopes of houses and consequent insurance losses." *J. Wind Eng. Ind. Aerodyn.* 53 (1–2): 145–155. https://doi.org/10.1016/0167-6105(94)90023-X.

Stewart, M. G., J. D. Ginger, D. J. Henderson, and P. C. Ryan. 2018. "Fragility and climate impact assessment of contemporary housing roof sheeting failure due to extreme wind." *Eng. Struct.* 171 (Sep): 464–475. https://doi.org/10.1016/j.engstruct.2018.05.125.

van de Lindt, J. W., and T. N. Dao. 2009. "Performance-based wind engineering for wood-frame buildings." *J. Struct. Eng.* 135 (2): 169–177. https://doi.org/10.1061/(ASCE)0733-9445(2009)135:2(169).

Vickery, P. J., P. F. Skerlj, J. Lin, L. A. Twisdale Jr., M. A. Young, and F. M. Lavelle. 2006. "HAZUS-MH hurricane model methodology. II: Damage and loss estimation." *Nat. Hazard. Rev.* 7 (2): 94–103. https://doi.org/10.1061/(ASCE)1527-6988(2006)7:2(94).

Wang, D., R. A. Davidson, L. K. Nozick, J. E. Trainor, and J. L. Kruse. 2020. "Computational framework to support government policy-making for hurricane risk management." *Nat. Hazard. Rev.* 21 (1): 04019012. https://doi.org/10.1061/(ASCE)NH.1527-6996.0000348.

Zillow. 2020. "ZTRAX: Zillow transaction and assessor dataset, 2020-Q3." Accessed December 8, 2021. https://www.zillow.com/ztrax/.